Harmonic-phase path-integral approximation of thermal quantum correlation functions

Christopher Robertson[a)] and Scott Habershon[a)]
Department of Chemistry and Centre for Scientific Computing, University Of Warwick, Coventry CV4 7AL, United Kingdom

(Received 30 August 2017; accepted 9 October 2017; published online 10 November 2017)

We present an approximation to the thermal symmetric form of the quantum time-correlation function in the standard position path-integral representation. By transforming to a sum-and-difference position representation and then Taylor-expanding the potential energy surface of the system to second order, the resulting expression provides a harmonic weighting function that approximately recovers the contribution of the phase to the time-correlation function. This method is readily implemented in a Monte Carlo sampling scheme and provides exact results for harmonic potentials (for both linear and non-linear operators) and near-quantitative results for anharmonic systems for low temperatures and times that are likely to be relevant to condensed phase experiments. This article focuses on one-dimensional examples to provide insights into convergence and sampling properties, and we also discuss how this approximation method may be extended to many-dimensional systems. *Published by AIP Publishing.* https://doi.org/10.1063/1.5002189

I. INTRODUCTION

Algorithms that employ the path-integral formulation of quantum statistical mechanics[1–4] have become invaluable tools for calculating time-independent thermal expectation values of quantum-mechanical operators, bridging the gap between the exponential-scaling wavefunction propagation methods and purely classical approaches for estimating thermodynamic observables. To date, path-integral molecular dynamics (PIMD) and path-integral Monte Carlo (PIMC) have been used to study quantum contributions to time-independent thermal equilibrium properties for a wide range of condensed-phase systems.[4–21] However, while *exact* time-independent properties can be calculated readily by PIMC or PIMD, path-integral evaluation of time-correlation functions (TCFs), allowing calculation of *time-dependent* properties, such as diffusion coefficients, scattering cross sections, dipole relaxation times, and reaction rates, remains an enormous challenge, principally as a result of the appearance of the so-called "sign problem" arising due to the action of quantum time propagators.[20,22–49]

Rather than seeking to address the sign problem directly, several successful simulation methods have shown that, for many systems, quantum dynamical properties can be well-approximated by assuming that explicit quantum coherent effects are "washed out" by the thermal environment, with the main quantum effect arising due to statistical fluctuations associated with zero-point energy (ZPE) conservation and tunneling. In this vein, methods such as ring-polymer molecular dynamics (RPMD[8,11,27,33,50–70]), centroid molecular dynamics (CMD[20,35,37,38,71–73]), and the linearised semi-classical initial value representation (LSC-IVR[42,43,45,48,49,74–77]) have proven to be enormously successful in modeling dynamic properties (via approximation of time-correlation functions) in a variety of condensed-phase systems represented by both model Hamiltonians and more accurate *ab initio* methods.

While methods such as RPMD, CMD, and LSC-IVR are appealing, principally due to both their physically consistent predictions and computational tractability, these approximations are not universally applicable. For example, it is well-known that RPMD time-correlation functions can exhibit spurious non-physical vibrational spectra,[27,38,57] and the associated treatment of non-linear operators is similarly challenging;[65] it is worth noting that these problems have been dramatically reduced by the recent introduction of thermostated RPMD (TRPMD[78]), although the introduction of an artificial broadening into associated vibrational spectra demonstrates that this approach is not a "cure-all." Similarly, vibrational spectra calculated by CMD can exhibit the so-called "curvature problem,"[38] while methods based on propagation of classical trajectories, such as LSC-IVR, can demonstrate the "ZPE-leakage problem."[57] Finally, in all cases (RPMD, CMD, and LSC-IVR), the neglect of explicit quantum coherence suggests that treatment of systems where this feature is prominent (e.g., coupled nuclear-electronic dynamics) remains challenging (although it is worth highlighting that progress is being made in this direction too[33,53,79]).

In this article, we present a further path-integral-based approximation of thermal quantum time-correlation functions that shows some promise for treating systems where explicit quantum phase interference might be important. Taking inspiration from much of the previous work on using Monte Carlo approaches to sample real-time quantum dynamics, we start from the symmetrized complex form of the quantum time-correlation function in the standard position path-integral

[a)]Electronic addresses: C.Robertson@warwick.ac.uk and S.Habershon@warwick.ac.uk

representation. In calculating the TCF, we transform the system coordinates to a sum-and- difference representation and subsequently Taylor-expand the potential energy of the system to second order around the "sum" path; in other words, we make a harmonic assumption for the potential energy surface in the "difference" coordinates. This approach enables one to explicitly evaluate the TCF integral over the "difference" coordinates. The resulting expression for the TCF provides one with a weighting function that approximately recovers the contribution of the phase to the TCF integral and which lies near the configurational space associated with the minimisation of the action. We show that under the harmonic assumption noted above, this approximation can adequately calculate TCF for anharmonic potentials. We refer to this approach as harmonic-phase approximation Monte Carlo (HPA-MC).

We note that our approach is similar to some already existing in the literature[22] but has some advantages; for example, HPA-MC does not require averaging over complex phases, as in recent approaches such as the partially linearised density matrix method.[80] Furthermore, HPA-MC does not require propagation of classical trajectories (and the inevitable ZPE leakage problem); in fact, as noted above, exact treatment of the Boltzmann operator is built into our approach (although the harmonic approximation in calculation of the TCF inevitably introduces errors, as discussed later). We note that HPA-MC gives the exact result for any harmonic system, for any operator; the non-linear operator problems which can appear in RPMD and CMD do not operate in HPA-MC. Importantly, we also find that HPA-MC can provide near-quantitative results for anharmonic PESs (Sec. II C) for low temperatures. It, nevertheless, suffers from accumulation of errors which only allows one to adequately approximate TCF for moderate real-times. The times and temperatures treated here are nevertheless relevant to condensed phase systems, and HPA-MC might prove to be an efficient approach for calculating transport properties for these. We conclude this article with a discussion of how HPA-MC might be improved upon and extended to higher-dimensional systems, work which is currently ongoing.

II. THEORY

We begin by briefly outlining the main concepts relating to quantum time-correlation functions which are relevant to this work. Then, we discuss the origin of the HPA-MC approach, before highlighting how this approach can enable efficient approximation of TCFs.

A. Quantum time-correlation functions

The standard quantum time-correlation function for two operators $\hat{A}$ and $\hat{B}$ is given by

$$C_{AB}(t) = \frac{1}{Z}\mathrm{Tr}\left[e^{-\beta\hat{H}}\hat{A}e^{+i\hat{H}t/\hbar}\hat{B}e^{-i\hat{H}t/\hbar}\right], \tag{1}$$

where $\beta = 1/(k_bT)$, Z is the partition function, and $\hat{H}$ is the Hamiltonian for the system, assumed throughout to be of the standard form $\hat{H} = \hat{T}+\hat{V}$, where $\hat{T}$ is the nuclear kinetic energy operator and $\hat{V}$ is the potential energy operator. Straightforward application of the path-integral approach to evaluate both imaginary-time and real-time propagator matrix elements results in an expression which requires averaging over a complex phase-factor, leading to the usual "sign problem."

An alternative TCF which is more amenable to MC integration is obtained by replacing $t \rightarrow t + i\beta\hbar/2$, giving the thermal symmetric TCF of the form,[81]

$$\begin{aligned} G_{AB}(t) &= C_{AB}(t + i\beta\hbar/2) \\ &= \frac{1}{Z}\mathrm{Tr}\left[\hat{A}e^{+i\hat{H}\tau^*/\hbar}\hat{B}e^{-i\hat{H}\tau/\hbar}\right], \end{aligned} \tag{2}$$

where $\tau = t - i\beta\hbar/2$. The two correlation functions $G_{AB}(t)$ and $C_{AB}(t)$ are related through their Fourier transforms such that $G_{AB}(\omega) = e^{-\beta\hbar/2}C_{AB}(\omega)$.

In $G_{AB}(t)$, the propagator elements $\langle x|e^{-i\hat{H}\tau^*/\hbar}|x'\rangle$ and $\langle x'|e^{-i\hat{H}\tau/\hbar}|x\rangle$ are complex conjugates, resulting in a real, positive-definite sampling function which enables MC integration. A number of approaches have shown this to be a fruitful avenue towards semiclassical approaches.[22,82] Specifically, the path-integral form of $G_{AB}(t)$ is[83]

$$\begin{aligned} G_{AB,P}(t) &= \frac{1}{Z}\int dx_1 \ldots dx_{2P}\, A(x_1)B(x_{P+1})\rho(x_1,\ldots,x_{2P})e^{i\Phi(x_1,\ldots,x_{2P})}, \\ \rho(x_1,\ldots,x_{2P}) &= \left(\frac{mP}{2\pi|\tau|\hbar}\right)^P \exp\left[-\frac{mP\beta}{4|\tau|^2\hbar^2}\sum_{k=1}^{2P}(x_{k+1}-x_k)^2 - \frac{\beta}{2P}\sum_{k=1}^{2P}V(x_k)\right], \\ \Phi(x_1,\ldots,x_{2P}) &= \frac{mPt}{2\hbar|\tau|^2}\left[\sum_{k=1}^{P}(x_{k+1}-x_k)^2 - \sum_{k=P+1}^{2P}(x_{k+1}-x_k)^2\right] - \frac{t}{\hbar P}\left[\sum_{k=2}^{P}V(x_k) - \sum_{k=P+2}^{2P}V(x_k)\right]. \end{aligned} \tag{3}$$

In Eq. (3) (and hereafter), we restrict our attention to one-dimensional systems for notational convenience; furthermore, we have assumed that each propagator matrix element in Eq. (2) has been discretised into P "slices," leading to $2P$ "slices" (or beads) to be sampled in total. The function $\rho(\mathbf{x})$ defines a sampling function for the coordinates of a ring-polymer under the influence of the PES and can be used to perform MC/MD estimation of G_{AB}[23] *via*

$$G_{AB}(t) = \frac{\langle A(x_1)B(x_{P+1})e^{i\Phi}\rangle_\rho}{\langle e^{i\Phi}\rangle_\rho}, \tag{4}$$

where $\langle\ldots\rangle_\rho$ implies averaging over the distribution $\rho(\mathbf{x})$. Unfortunately, estimating $G_{AB}(t)$ based on sampling from ρ

gives rise to known difficulties, and a number of strategies have been devised to attempt to improve the convergence.[30,82,84,85] Averaging over $e^{i\Phi}$ gives rise to both positive and negative contributions (i.e., appearance of the "sign problem"), and the denominator can approach zero for long times, making the integrals difficult to converge using standard simulation methods.

B. Harmonic-phase approximation

To escape the difficulties noted above, our approach is, to substitute $e^{i\Phi}$ by a function, based on a harmonic approximation, which approximately provides the correct weighting to a particular path, avoiding the highly oscillatory behaviour. To proceed, we turn to a "sum and difference" representation using the coordinates of adjacent "beads" along the forward and backward paths which emerge upon path-integral treatment of the propagator matrix elements (Fig. 1). Here, let $x'_i = x_{2P+2-i}, 2 \le i \le P$. A general orthogonal transformation of x'_i and x_i that maintains a phase-space area must satisfy the following constraint in the Jacobian,

$$\begin{vmatrix} \frac{dx}{dx^+} & \frac{dx}{dx^-} \\ \frac{dx'}{dx^+} & \frac{dx'}{dx^-} \end{vmatrix} = \begin{vmatrix} a & -b \\ a & b \end{vmatrix} = 1. \tag{5}$$

Such transformations are given by

$$\begin{aligned} x &= ax^+ + (1/2a)x^-, \qquad x^+ = \frac{1}{2a}(x + x'), \\ x' &= ax^+ - (1/2a)x^-, \qquad x^- = a(x - x'), \end{aligned} \tag{6}$$

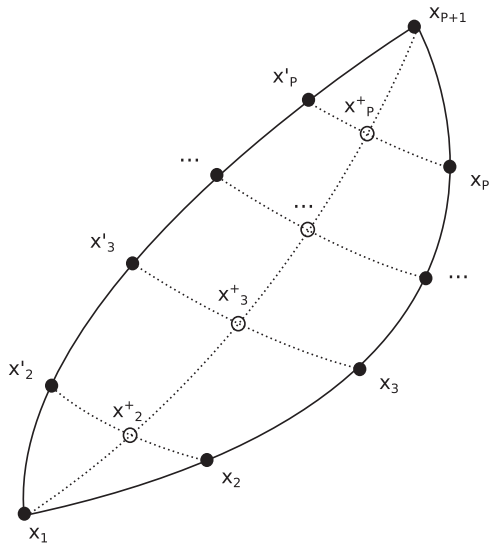

FIG. 1. Diagram showing the ring representing the forward and backward paths: $\{x, x'\}$ beads are indexed in accord to their position away from bead x_1 and rotated to obtain x^+, the sum coordinates (the mean, if $a = 1$). x^- not displayed.

where a and b are fixed constants, and we refer to the x^+ as "sum" coordinates and x^- as "difference" coordinates. For notational convenience, we define $x^+_1 = x_1$ and $x^+_{P+1} = x_{P+1}$.

Transforming to these new coordinates, the density and phase of Eq. (3) (omitting irrelevant pre-exponential factors) are now

$$\begin{aligned} \rho(x^+_1,\ldots,x^+_{P+1},x^-_2,\ldots,x^-_P) = \exp\Bigg[-\frac{mP\beta}{4|\tau|^2\hbar^2}\Bigg\{2((x^+_1 - ax^+_2)^2 + (x^+_{P+1} - ax^+_P)^2 + a^2\sum_{k=2}^{P-1}(x^+_k - x^+_{k+1})^2) \\ + \frac{1}{2a^2}((x^-_2)^2 + (x^-_P)^2 + \sum_{k=2}^{P-1}(x^-_k - x^-_{k+1})^2)\Bigg\} - \frac{\beta}{2P}\Bigg\{V(x^+_1) + V(x^+_{P+1}) \\ + \sum_{k=2}^{P-1} V(ax^+_k + (1/2a)x^-_k) + V(ax^+_k - (1/2a)x^-_k)\Bigg\}\Bigg], \\ \Phi(x^+_1,\ldots,x^+_{P+1},x^-_2,\ldots,x^-_P) = \frac{mPt}{\hbar|\tau|^2}\Bigg[x^+_2x^-_2 + x^+_Px^-_P - \frac{1}{a}(x^-_2x^+_1 + x^-_Px^+_{P+1}) + \sum_{k=2}^{P-1}(x^+_{k+1} - x^+_k)(x^-_{k+1} - x^-_k) \\ - \frac{t}{\hbar P}(\sum_{k=2}^{P} V(ax^+_k + (1/2a)x^-_k) - V(ax^+_k - (1/2a)x^-_k))\Bigg]. \end{aligned} \tag{7}$$

Equation (7) shows that the sum coordinates $\mathbf{x}^+$ describe the average discretised path as a string coupled to the difference string defined by $\mathbf{x}^-$.

To proceed, we now Taylor-expand the PES appearing in both the phase and the density about $a\mathbf{x}^+$, such that

$$V(x) \approx V(ax^+) + \left(\frac{x^-}{2a}\right)\frac{\partial V}{\partial x}\bigg|_{x\,=ax^+} + \frac{1}{2}\left(\frac{x^-}{2a}\right)^2\frac{\partial^2 V}{\partial x^2}\bigg|_{x=ax^+}. \tag{8}$$

Noting that the PES at identically labelled beads, k appears in Eq. (7) as either a sum (in the case of density) or a difference (in the case of the phase), we find that

$$\begin{aligned} V(x) + V(x') &\approx 2V(ax^+) + \frac{(x^-)^2}{4a^2}\frac{\partial^2 V}{\partial x^2}\bigg|_{x=ax^+}, \\ V(x) - V(x') &\approx \left(\frac{x^-}{a}\right)\frac{\partial V}{\partial x}\bigg|_{x=ax^+}. \end{aligned} \tag{9}$$

Substituting these approximations into Eq. (7), we see that all even orders of $\mathbf{x}^-$ cancel out in the phase-factor Φ and

all odd orders of x^- cancel out in the density ρ. Notice that for any choice of a, all derivatives $\frac{\partial^n V}{\partial x^n}|_{x=ax^+}$ are evaluated at the mean of the two beads, since $ax^+ = a(\frac{1}{2a}(x + x')) = (\frac{1}{2}(x + x'))$. We shall nevertheless find it convenient to use $a = 1/\sqrt{2}$ when analysing the harmonic oscillator case (see the Appendix). We note that the transformation and second-order expansion performed so far remain exact for any harmonic PES. It can also be shown that for a cubic PES, a term is lost in the phase component, and for a quartic PES, terms in the phase and density parts are lost. For convenience, we now denote $\frac{\partial^n V}{\partial x^n}|_{x=ax^+} = \frac{\partial^n V^+}{\partial x^n}$.

The upshot of this coordinate transformation and expansion is that the thermal symmetric TCF can be written as

$$G_{AB}(t) = \frac{1}{Z}\int d\mathbf{x}^+\, d\mathbf{x}^-\rho^+(\mathbf{x}^+)\rho^-(\mathbf{x}^-)A(x_1)B(x_{P+1})e^{i\Phi'(\mathbf{x}^+,\mathbf{x}^-)}. \tag{10}$$

The "sum bead" contribution to the density is given by

$$\ln(\rho^+) = \frac{-m\beta P a^2}{|\tau|^2\hbar^2}\left\{\frac{1}{2a^2}((x_1^+)^2 + (x_{p+1}^+)^2) + (x_p^+)^2 - \frac{1}{a}(x_{p+1}^+x_p^+ + x_1^+x_2^+) + \sum_{k=2}^{P-1}(x_k^+)^2 - x_k^+x_{k+1}^+ + \frac{|\tau|^2\hbar^2}{2ma^2P^2}\left(V(x_1^+) + V(x_{P+1}^+) + 2\sum_{k=2}^{P}V(ax_k^+)\right)\right\}. \tag{11}$$

Thus, $\rho^+(\mathbf{x}^+)$ provides a configurational sampling function which can be sampled by MC in a similar manner to the standard PIMC methodology, with the exception that $\rho(\mathbf{x}^+)$ describes a "string polymer" rather than a "ring polymer." Furthermore, the spring constants of Eq. (11) depend on both the inverse temperature β and the real time t, again in contrast to the standard PIMC/PIMD approach.

At this point, we do not appear to have made much progress in achieving a computationally tractable scheme when compared to Eq. (4). We would still have to sample configurations from $\rho^+\rho^-$ and the 'sign problem' $e^{i\Phi'}$ remains. However, we now show that the coordinate transformation and harmonic expansion noted above enable one to analytically integrate out the dependence on the $\mathbf{x}^-$ coordinates, thereby removing the oscillatory nature of the integrand.

First, we note that that "difference bead" contribution to the density is given by

$$\ln(\rho^-(\mathbf{x}^-)) = \frac{-m\beta P}{4\hbar^2|\tau|^2a^2}\left\{(x_p^-)^2 + \sum_{k=2}^{P-1}(x_k^-)^2 - x_k^-x_{k+1}^- + \frac{|\tau|^2\hbar^2}{2mP^2}\sum_{k=2}^{P}(x_k^-)^2\frac{\partial^2V^+}{\partial x_k^2}\right\}. \tag{12}$$

Twice differentiating this term gives an effective "Hessian" matrix for the difference string (omitting common factors) of the form

$$\mathbf{H}'^- = \mathbf{H}^- + \frac{|\tau|^2\hbar^2}{mP^2}1\!\!1\frac{\partial^2\vec{V}^+}{\partial x^2} = \begin{pmatrix} 2 & -1 & 0 & \cdots \\ -1 & 2 & -1 & \\ 0 & -1 & 2 & \\ \vdots & & & \ddots \end{pmatrix} + \frac{|\tau|^2\hbar^2}{mP^2}1\!\!1\frac{\partial^2\vec{V}^+}{\partial x^2}. \tag{13}$$

The first matrix in Eq. (13), $\mathbf{H}^-$, has analytical eigenvectors and eigenvalues of the form

$$U_{ij}^- = \sqrt{\frac{2}{P}}\sin\left(\frac{\pi(i-1)(j-1)}{P}\right), \qquad (\lambda_i^-)^2 = 4\sin^2\left(\frac{\pi(i-1)}{2P}\right). \tag{14}$$

For general quadratic potentials of the form $\omega_r^2x^2$, the eigenvalues of Eq. (14) have to be modified with the addition of the force constant $\frac{2\omega_r^2|\tau|^2\hbar^2}{mP^2}$. For higher-order potentials, we would need to directly diagonalise the tridiagonal matrix $\mathbf{H}'^-$ as a function of $\vec{x}^+$ (see later for discussion), and $\mathbf{U}'^-$ would no longer be symmetric.

Next, we note that phase factor in Eq. (10) is given by

$$\Phi' = \frac{Ptm}{\hbar|\tau|^2}\left[\left\{(x_2^+)(x_2^-) - (x_2^-)(x_1)/a + (x_p^+)(x_p^-) - (x_{p+1})(x_p^-)/a + \sum_{k=2}^{P-1}(x_{k+1}^+ - x_k^+)(x_{k+1}^- - x_k^-)\right\} - \frac{t}{\hbar P}\sum_{k=2}^{P}(\frac{x_k^-}{a})\frac{\partial V^+}{\partial x_k}\right]. \tag{15}$$

We then note that each difference coordinate x_k^- has an associated constant c_k^+ such that we can write

$$\Phi' = \frac{Ptm}{\hbar|\tau|^2}\sum_{k,i=2}^{P}x_k^-c_k^+, \tag{16}$$

where

$$c_k^+ = \left[\{(2x_k^+ - (\alpha x_{k-1}^+ + \gamma x_{k+1}^+)\} - \frac{|\tau|^2}{aP^2m}\frac{\partial V^+}{\partial x_k}\right], \qquad \begin{cases}\alpha = 1/a, & k-1=1\\ \alpha = 1, & k-1>1\\ \gamma = 1/a, & k+1=P\\ \gamma = 1, & k+1<P\end{cases}. \tag{17}$$

We now transform to a normal-mode representation in the difference coordinates only, using the Hessian associated with the difference density $\rho^-(\mathbf{x}^-)$. The required transformation is given by $\mathbf{x}^- = \mathbf{U}'^-\mathbf{q}^-$, so that

$$\Phi' = \frac{Ptm}{\hbar|\tau|^2}\sum_{k,i=2}^{P}U'^-_{ki}q_i^-c_k^+ = \frac{Ptm}{\hbar|\tau|^2}\sum_{k,i=2}^{P}q_i^-U'^-_{ki}c_k^+. \tag{18}$$

We define $C_k^+ = \sum_{i=2}^{P}U'^-_{ik}c_i^+$, and $(\lambda_k'^-)^2$ defines the eigenvalues of $\mathbf{H}^-$ including the diagonal $\frac{|\tau|^2\hbar^2}{mP^2}\frac{\partial^2V^+}{\partial x_k^2}$ contributions [Eq. (13)]. Under this normal-mode transformation, the integral of $\mathbf{x}^-$ (or, equivalently, $\mathbf{q}^-$) in Eq. (10) can now be performed analytically as follows:

$$F^-(\mathbf{x}^+) = \int d\mathbf{q}^- \rho^- e^{i\Phi'} = \int dq_2^- \cdots dq_p^- \exp\left[\frac{-m\beta P}{8\hbar^2|\tau|^2 a^2}\sum_{k=2}^{P}(\lambda_k'^-)^2(q_k^-)^2\right]\exp\left[i\frac{Ptm}{\hbar|\tau|^2}\sum_{k=2}^{P}q_k^- C_k^+\right]$$
$$= \prod_{k=2}^{P}\sqrt{\frac{8\hbar^2\pi a^2|\tau|^2}{P\beta m(\lambda_k'^-)^2}}\exp\left[-\frac{2ma^2t^2P}{|\tau|^2\beta}\sum_{k=2}^{P}(\frac{C_k^+}{\lambda_k'^-})^2\right], \tag{19}$$

where, in the second line of Eq. (19), we have used the standard Fourier transformation of a Gaussian function. The integral over ρ^- and the phase factor have now been replaced by a simple Gaussian function $F^-(\mathbf{x}^+)$ that depends on x^+ and derivatives of the potential energy surface with respect to these coordinates. Thus, the TCF of Eq. (10) can be written as

$$G_{AB}(t) = \frac{1}{Z}\int d\mathbf{x}^+ [\rho^+(\mathbf{x}^+)F^-(\mathbf{x}^+)]A(x_1)B(x_{P+1}), \tag{20}$$

such that, under the harmonic approximation of the PES, $G_{AB}(t)$ can be calculated by MC sampling from $\rho^+(\mathbf{x}^+)F^-(\mathbf{x}^+)$. In passing, we note that the width of the Gaussian function $F^-(\mathbf{x}^+)$ depends on the different Hessian eigenvalues $(\lambda_k'^-)^2$. Interestingly, identifying the maximum of this Gaussian function yields the condition (assuming here that $a = 1$),

$$x_{k+1}^+ = 2x_k^+ - x_{k-1}^+ - \frac{|\tau|^2}{P^2 m}\frac{\partial V^+}{\partial x_k}, \tag{21}$$

which can be seen to be the Verlet algorithm for propagation of a classical trajectory, with an additional force contributed by the inverse temperature (which would disappear in the usual high-temperature classical limit). This result can be contrasted to the resulting expression obtained when applying an analogous treatment to the purely real-time TCF,[86] where one obtains a delta function, as opposed to a Gaussian, determining a classical evolution. One can show that the exponent in the second line of Eq. (19) can be re-written as (see the Appendix)

$$x_\gamma^+\left(d_{i\gamma} - \frac{|\tau|^2}{P^2 m}\frac{\partial V^+}{\partial x_\gamma}\delta_{i\gamma}\right)((H^-)_{ij}^{-1})\left(d_{j\kappa} - \frac{|\tau|^2}{P^2 m}\frac{\partial V^+}{\partial x_\kappa}\delta_{j\kappa}\right)x_\alpha^+,$$
$$d_{ki} = \begin{cases} 2, & i = k \\ -\alpha, & i = k-1 \\ -\gamma, & i = k+1 \\ 0, & |i-k| > 1 \end{cases}, \quad \alpha = \begin{cases} 1/a, & i = 1 \\ 1, & i > 1 \end{cases}, \quad \gamma = \begin{cases} 1/a, & i = P+1 \\ 1, & i < P+1, \end{cases} \tag{22}$$

where indices i, j refer to the difference degrees of freedom and $(H^-)^{-1}$ is defined in Eq. (13). The outer brackets correspond to a Verlet step along some sum coordinate x_κ^+ approximately describing a classical path. An implication is that any $x_{\kappa+1}^+$ bead will depend upon the "history" of the trajectory defined by all the other beads.

C. Treating anharmonic PESs

For a general (anharmonic) PES, Eq. (20) is not applicable. In particular, the integral over the difference coordinate, x^-, in Eq. (19) cannot be performed exactly because, in general, the PES is no longer exactly separable when transformed to sum-and-difference coordinates. We are forced to retain a second-order expansion on the density since Fourier transform of negative exponentials with higher than quadratic functions does not have simple analytic forms. Similarly we are forced to retain a linearisation of the phase since a cubic term would no longer allow one to easily perform a Fourier transformation. As mentioned in Sec. II B, for a harmonic system, the coordinates x_1 and x_{P+1} are only coupled to the negative beads via the phase, which integrates onto a Gaussian which is a function of the x^+ derivatives of the potential. In other words, the density contribution was correctly sampled by ρ^+ and the phase contribution by $\int dx^- \rho^- e^{i\Phi} = F^-$. For anharmonic systems, the truncated ρ^+ will not sample the correct Boltzmann distribution and therefore cannot be used to provide accurate approximations to the integral.

Instead, the HPA-MC approximation which we arrive at for general anharmonic potential energy surfaces uses Eq. (20) to calculate the correlation function, but instead of sampling $\mathbf{x}^+$ from ρ^+, we sample directly from the original path-integral density given by ρ in Eq. (3). The $\mathbf{x}^\pm$ coordinates sampled by this approach are then used directly in the calculation of F^-, the explicit expression for which is

$$\ln(F^-) = -\frac{2ma^2t^2P}{|\tau|^2\beta}\sum_{k=2}^{P}\frac{\left[\sum_{i=2}^{P}U'^-_{ki}\sum_{j=1}^{P+1}(d_{ij} - \frac{|\tau|^2}{amP^2}\frac{\partial V^+}{\partial x_i}\delta_{ij})x_j^+\right]^2}{\sum_{i,j=2}^{P}U'^-_{ki}(H_{ij}^- + \frac{|\tau|^2\hbar^2}{mP^2}\frac{\partial^2 V^+}{\partial x_i^2}\delta_{ij})U'^-_{kj}}, \quad d_{ij} = \begin{cases} 2, & i = j \\ -\alpha, & i = j-1 \\ -\gamma, & i = j+1 \\ 0, & |i-j| > 1 \end{cases}, \quad \alpha = \begin{cases} 1/a, & i = 1, \\ 1 & i > 1 \end{cases}, \quad \gamma = \begin{cases} 1/a, & i = P+1 \\ 1, & i < P+1, \end{cases} \tag{23}$$

where the denominator shows $(\lambda'^-)^2$ in the sum/difference representation to show the dependence on second derivatives. F^- corresponds to the weight the phase would contribute if at every given configuration the system potential was truncated to second order and $\int dx^- \rho^- e^{i\Phi'}$ integrated, which clearly gives the exact result for harmonic potential. We shall show that better results are obtained if we use interpolated values for $\frac{\partial^{|1|2}V^+}{\partial x^{1|2}}$ from the derivatives and energies sampled from ρ, under the assumption that the underlying potential interpolated is harmonic.

III. APPLICATIONS AND RESULTS

To test HPA-MC, we focus on calculating time-correlation functions for one-dimensional systems where the operators of interest are linear or non-linear position operators. We focus on two particular model systems which have been used extensively to benchmark other quantum simulation methods:[22,40,41,52,82,87]

$$V(x) = \frac{1}{2}x^2 + \frac{1}{10}x^3 + \frac{1}{100}x^4,$$
$$V(x) = \frac{1}{4}x^4. \tag{24}$$

We refer to these two systems as the "mildly" and "strongly anharmonic" problems, respectively. As we have already noted, for a harmonic potential, $V(x) = \frac{m\omega^2}{2}x^2$, the HPA-MC approach outlined above is exact, assuming that an appropriate number of path-integral beads (P) is employed during sampling (see the Appendix for errors associated with the limited number of beads). We note that this applies equally to TCFs of both linear *and* non-linear operators, in contrast to methods such as RPMD and CMD, which can exhibit pathological errors when calculating correlation functions for non-linear operators. Furthermore, based on numerical analysis of the integral in Eq. (20), it is possible to identify an approximate condition on the requisite number of beads for a given time t required for convergence; this is discussed in detail in the Appendix. So, we focus here on the application of HPA-MC to the calculation of TCFs for anharmonic PESs; first, we discuss a particularly efficient implementation of HPA-MC, and then we illustrate the performance of our approach to model anharmonic problems which test when this methodology is expected to work.

A. Improving Monte Carlo sampling using a harmonic-phase normal representation

We shall briefly discuss implementation of the Monte-Carlo M(RT)^2 algorithm.[83] Performing MC steps in a standard Cartesian coordinate representation inevitably leads to poor convergence, getting progressively worse for longer real-times. This is, in part, explained by the denominator in Eq. (23), for which eigenvalues $(\lambda_k'^-)^2$ close to zero give rise to a sharp distribution; as a result, large Cartesian displacements inevitably have a low probability of acceptance, meaning that sampling of configurational space is slow. However, it is possible to develop a considerably better representation which gives a reasonably consistent MC acceptance ratio for any time and many types of anharmonic systems.

First, we can obtain an effective harmonic force constant for the full PES (for some inverse temperature β). For a harmonic oscillator, the exponent of the density normal-mode representation is

$$\frac{mP\beta}{4\hbar^2|\tau|^2}\sum_i^{2P}\left\{\lambda_i^2 + \frac{2\hbar^2|\tau|^2}{mP^2}\omega_s^2\right\}\frac{q_i^2}{2}, \tag{25}$$

with a standard deviation for each mode i given by

$$\sigma_i(\omega_s) = \left[\frac{mP\beta}{4\hbar^2|\tau|^2}\left\{\lambda_i^2 + \frac{2\hbar^2|\tau|^2}{mP^2}\omega_s^2\right\}\right]^{-\frac{1}{2}}. \tag{26}$$

A trial probability function given by $\pm 3\xi\sigma_i$ along any mode, where ξ is a uniform distribution between $-\frac{1}{2} < \xi < \frac{1}{2}$, should result in an equal pass/fail ratio of $\sim \frac{1}{2}$. For a general potential, we can obtain an effective harmonic constant by optimising ω_{eff} (in place of ω_s^2) such that the difference between the pass/fail ratio given by $\sigma_0(\omega_{eff})$, the centroid of the ring's normal coordinate, and the other modes $[\sigma_i(\omega_{eff})]$ is minimised when performing MC at $t = 0$. This temperature-dependent effective frequency can then be used to obtain a normal-mode representation of the matrix in Eq. (A2) (using the effective ω_{eff} in place of ω) but with the inclusion of the ring Hessian,

$$(\mathbf{x})^T\mathbf{R}'^T\mathbf{R}'\left(\frac{\beta mP}{2\hbar^2\tau^2}\mathbf{H} + 2\varphi\right)\mathbf{R}'^T\mathbf{R}'\mathbf{x} = \mathbf{q}'^T\Lambda\mathbf{q}', \tag{27}$$

where $\varphi = \ln(F^-)$. With the transformation $\mathbf{R}'$, a second effective harmonic frequency is then obtained by performing the same optimisation as before but this time using the effective normal-mode representation q'. This new effective frequency can then be used together with the q' representation to obtain a more consistent sampling for the particular time t. Though methods for reducing the variance of the sampling function, such as importance/umbrella sampling[88] or staging algorithms,[89] could be used to improve convergence, this "effective frequency optimisation" approach was sufficient for the purposes of this paper.

B. Harmonic interpolation of the HPA-MC for anharmonic potential

Second derivatives are required in the approximation given in Eq. (23). In practice, evaluating second derivatives $\frac{\partial^2 V^+}{\partial x_i^2}$ increases computational cost; as a result, in the anticipation of applying HPA-MC to more complex systems, we explore how this method can be implemented while avoiding explicit calculation of the Hessian. Several alternative approaches for approximating second-order derivatives can be devised, which give the correct derivatives for a harmonic oscillator; we investigate two of these in the simulations given below.

First, results calculated with analytical first derivatives and analytical Hessian will be labelled *E-fit*. A good choice for the interpolated first derivative is also the simplest: $(V(x) - V(x'))/(x - x')$, which is a simple numerical derivative at the ρ bead points. For the second derivatives, the first approximation we use is

$$\left.\frac{\partial^2 V}{\partial^2 x}\right|_{x=x^+} = \frac{V(x) - 2V(x^+) + V(x')}{(x - x')^2},$$

which is a central-difference numerical second derivative using only the potential energy; this approximation is labelled as *V-fit* in Figs. 2–4 below. The second approximation to second derivatives which we employ is

$$\left.\frac{\partial^2 V}{\partial^2 x}\right|_{x=x^+} = \frac{(\frac{\partial V}{\partial x}(x) - \frac{\partial V}{\partial x}(x'))}{(x - x')},$$

which will be referred to hereafter as *D-fit*. D/V-fit uses the aforementioned first derivative interpolation.

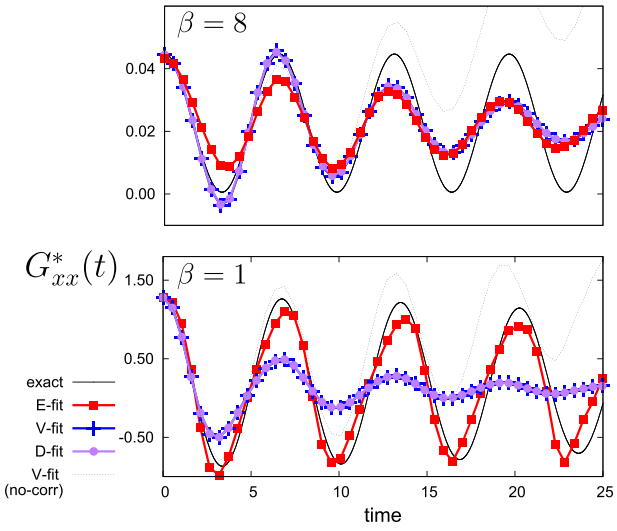

FIG. 2. G_{xx} for low ($\beta = 8$, *top panel*) and high ($\beta = 1$, *bottom panel*) temperatures for the mildly anharmonic model $\frac{1}{2}x^2 + \frac{1}{10}x^3 + \frac{1}{100}x^4$. Labels correspond to numerical derivatives for Eq. (23) explained in Subsection III B. The dashed line corresponds to not using the correction of Eq. (28). In black, we show the exact quantum mechanical results.

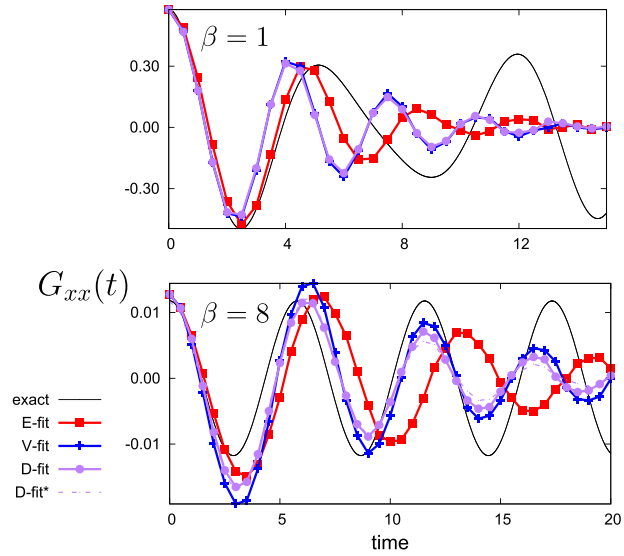

FIG. 4. G_{xx} for low ($\beta = 8$, *bottom panel*) and high ($\beta = 1$, *top panel*) temperatures for the strongly anharmonic model $\frac{1}{4}x^4$. Labels correspond to numerical derivatives for Eq. (23) explained in Subsection III B. D-fit* is the same as D-fit but using fixed number of beads through t, $P = 60$ (*bottom panel*). In black, we show the exact quantum mechanical results.

C. Anharmonic models at high and low temperatures

We tested the HPA-MC approximation for the anharmonic models given in Eq. (24), by computing $G_{xx}(t)$ and $G_{x^2x^2}(t)$ correlation functions at high ($\beta = 1$) and low ($\beta = 8$) temperatures. We used the numerical interpolations described above, D-fit, V-fit, and the exact derivatives E-fit. To ensure a small P source error (see the Appendix for more detailed discussion), we used a greater number of beads than that suggested by Eq. (A9). To use Eq. (A9), we took the effective harmonic force constant determined in the first step of the procedure described in Sec. III A [pertaining Eq. (26)], with a sufficiently converged number of beads.

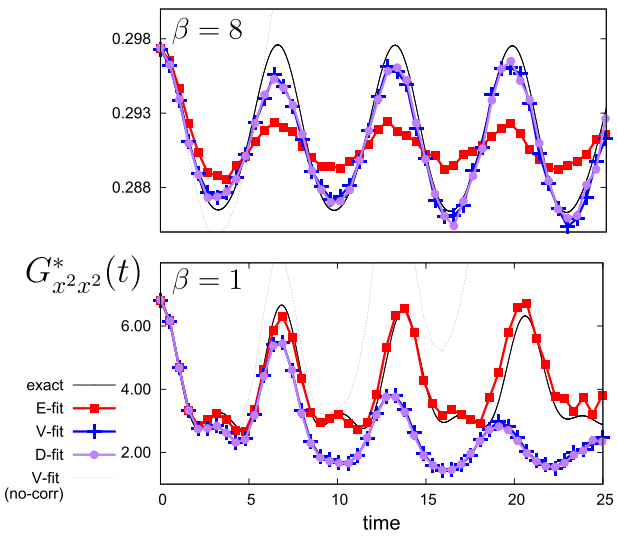

FIG. 3. $G_{x^2x^2}$ for low ($\beta = 8$, *top panel*) and high ($\beta = 1$, *bottom panel*) temperatures for the mildly anharmonic model $\frac{1}{2}x^2 + \frac{1}{10}x^3 + \frac{1}{100}x^4$. Labels correspond to numerical derivatives for Eq. (23) explained in Subsection III B. The dashed plot corresponds to not using the correction of Eq. (28). In black, we show the exact quantum mechanical results.

In Figs. 2 and 3, we show the results for $G_{xx}(t)$ and $G_{x^2x^2}(t)$ for the mildly anharmonic model at low and high temperatures. This model exhibits one of the main shortcomings of this approximation; for any potential with non-symmetric terms (i.e., $\frac{1}{10}x^3$), the correlation functions suffer from a monotonic growth in errors as a function of t, for any position correlation function [an analogous error also occurs for $G_{x^2x^2}(t)$ for the harmonic oscillator, which originates from the use of a small number of beads P (see the Appendix)]. In this case, however, increasing the number of beads does not eliminate this problem. Instead, this error arises because the HPA-MC phase factor F^-, which is included in the calculation of correlation functions and expectation values here, is an approximation and so introduces an error. However, because we know the correct expectation values (from exact PIMD or PIMC simulations at real-time $t = 0$), we can approximately correct this error by a simple, albeit *ad hoc* scaling. Specifically, because we know that expectation values should be independent of time, the following correction can be applied:

$$G^*_{xx}(t) = G_{xx}(t)\left(\frac{\langle x_1\rangle^2(t=0)}{\langle x_1\rangle^2(t)}\right),$$
$$G^*_{x^2x^2}(t) = G_{x^2x^2}(t)\left(\frac{\langle x_1^2\rangle^2(t=0)}{\langle x_1^2\rangle^2(t)}\right). \tag{28}$$

Since $\langle x_1^{1|2}\rangle$ converges quickly, this correction can be applied with little additional cost. To ensure a minimal error arising from the number of beads P, we used three times the suggested number by Eq. (A9). This resulted in $2P = 42$ beads at $t = 0$ and $2P = 128$ at $t = 25$.

For both Figs. 2 and 3, both numerical interpolations give similar results, suggesting that one can potentially avoid evaluating analytical derivatives completely. Calculation of exact derivatives (E-fit) generates a better approximation at high temperature but appears worse at low temperatures when compared to the interpolation results; this is in part a consequence

of the fact that the harmonic interpolated approximation of the potential energy surface will become increasingly inaccurate at higher temperatures (loosening of ring beads). The results for the interpolated approximations without the scaling of Eq. (28) are also shown, demonstrating monotonic growth in the error associated with propagation of the error in the harmonic approximation at longer times. It is also worth noting that for the exact derivatives this error is not present at high temperatures (the scaling factor is nevertheless used for E-fit in Figs. 2 and 3).

From the $G_{xx}(t)$ results in the top panel of Fig. 2 ($\beta = 8$), one can observe that, although the phase matches the exact results, the correction re-scaling has the unfortunate effect of reducing the amplitude of the oscillations, making the approach only feasible for moderate times. E-fit exhibits a smaller amplitude but appears to decay slower than the interpolated approximations. On a similar note, the monotonic growth in the error for E-fit is present but smaller than for the other two approximations (the dashed line shown in Fig. 2 is using V/D-fit). For the interpolated approximations, the problem is exacerbated further at high temperatures (bottom panel), with the amplitude decaying very rapidly when using the re-scaling of Eq. (28). In contrast, the exact derivative performs much better, with little decay over time.

Somewhat surprisingly, the interpolated approximations of $G_{x^2x^2}(t)$ for low temperatures $\beta = 8$ [Fig. 3 with the correction of Eq. (28)] do better at semiquantitatively maintaining the amplitude and phase to longer times. The exact derivative maintains the phase over the time shown, with an incorrect, smaller amplitude. The error growth is as severe as for the interpolated approximations. The convergence of these TCFs is much tougher to achieve than their corresponding odd-termed correlation functions (as discussed in Subsection III D).

The behaviour of the exact and interpolated methods could perhaps be rationalised by considering three key points. First, for anharmonic models, the use of the HPA factor $F^{-}(\mathbf{x}^{+})$ in the calculation of the correlation function will introduce an error; this factor is derived based on assuming a harmonic potential and cannot account for anharmonic terms. Second, at low temperatures, when the region of phase-space explored by the ring-polymer is expected to be confined to regions near the bottom of the PES, the harmonic interpolation of the PES might be expected to be quite accurate, particularly for mildly anharmonic systems; as a result, the error introduced by the HPA would be expected to be smaller. Third, at high temperatures (small β), the ring-polymer explores a larger degree of phase-space, including regions of significant anharmonicity; as a result, the HPA would be expected to become more inaccurate. Taken together, these comments suggest that interpolation methods such as V-fit and D-fit should work better at low temperatures (large β), whereas the E-fit method should work better at high temperatures. This trend is evident in Figs. 2 and 3.

For higher temperature, interpolated approximations (lower panel of Fig. 3), the scaling factor leads to an erroneous decay which only mildly fixes the error growth. The amplitude and phase are also mostly lost by 25 reduced units of time. In contrast, the exact derivative gives much better results over the time shown, with the scaling factor slightly improving the result. The fact that the interpolated approximations seem to give TCFs which decay with time suggests that the harmonic factor $F^{-}(\mathbf{x}^{+})$ calculated using interpolation is simply not sufficiently accurate at higher temperatures, where significant anharmonicity will be encountered; in this case, the rescaling procedure seems to over-damp the TCFs. In contrast, the exact derivatives (E-fit) result in a good approximation to the exact TCF. In this case, presumably because the calculated factor $F^{-}(\mathbf{x}^{+})$ in some way incorporates some of the effects of anharmonicity via the use of exact derivatives.

Next, Fig. 4 shows $G_{xx}(t)$ for the strongly anharmonic model (i.e., the quartic oscillator). For all cases, both the amplitude and phase are lost by 20 units of time, and the error begins within the first period. For the low temperature regime (bottom panel of Fig. 4), in all three instances, the first period is over-shot, but the overall frequency-increase and amplitude-decay errors gradually grow as time increases. The potential-only V-fit shows an excessive amplitude at short times, which is improved by the gradient, D-fit, interpolation. Unfortunately this improvement in D-fit also means that the amplitude approaches zero faster. The exact derivative results, E-fit, exhibit a longer period of oscillation but suffer less amplitude-decay or a frequency-increase error. Despite these shortcomings, the numerical derivative approximations exhibit semi-quantitative results for three periods before decaying. In contrast, results in the high-temperature regime ($\beta = 1$, top panel of Fig. 4) are much worse, exhibiting errors in frequency and amplitude by the end of the first period of oscillation. All information is lost by 15 units of time. The exact derivatives perform somewhat better than the numerical derivative cases. Similar poor behaviour is observed in other methods, such as RPMD/CMD.[83] The explanation given[58] in those methods is that long term oscillations on high temperature regimes arise from higher-order terms in the phase. Higher-order terms are also explicitly missing in this approximation. Since there is a qualitative resemblance between the poor performances of RPMD/CMD and HPA, these missing terms might also be the explanation here. We used four times the number of beads suggested by Eq. (A9). This resulted in $2P = 20$ at $t = 0$ and $2P = 124$ at $t = 20$. Nevertheless, more modest number of beads can be used to obtain similar results, with little decay of the amplitude. Converged results for $2P = 60$ in dashes for D-fit in the low temperature panel in Fig. 4 show that the quality of interpolation is not significantly affected by such choice of P. Nevertheless, a decrease in amplitude creeps in at slightly earlier times for smaller P, similar to the harmonic oscillator cases.

D. MC convergence

To get a feeling for the efficiency with which one can obtain converged HPA-MC results, we analyze the performance of this particular implementation of the M(RT)^2 algorithm by comparing the convergence of different $G_{x^m x^m}(t)$ correlation functions ($m = 1$, 2, or 3) for the harmonic $\frac{1}{8}x^2$ model, the mildly anharmonic model, and the strongly anharmonic model, using $2P = 80$, $\beta = 8$. Equations (A5) (Subsection 1 of the Appendix) allow one to calculate the exact variance in the

position and position-squared correlation functions as

$$\delta(x_1^1 x_{P+1}^1) = (\langle x_1^2 x_{P+1}^2\rangle - \langle x_1 x_{P+1}\rangle^2)^{\frac{1}{2}}$$

and

$$\delta(x_1^2 x_{P+1}^2) = (\langle x_1^4 x_{P+1}^4\rangle - \langle x_1^2 x_{P+1}^2\rangle^2)^{\frac{1}{2}}$$

for the harmonic oscillator potential. The central limit theorem can approximately suggest the *relative* cost of convergence using an idealised Monte-Carlo integrator. For the system parameters $2P = 80$, $\beta = 8$, $t = \pi$ (time for which $\langle x_1 x_{P+1}\rangle^2 = 0$), we get $\delta(x_1^1 x_{P+1}^1) \approx 1$ and $\delta(x_1^2 x_{P+1}^2) \approx 3$, suggesting that it would be more expensive by nearly a factor of three to reduce the error in the correlation function involving x^2 to the same value as the correlation function for just x. If a relatively small number of beads is chosen such that the monotonically increasing error due to P observed for $G_{x^2x^2}(t)$ (Appendix) occurs at small t, the central limit theorem suggests that $G_{xx}(t)$ will also become harder to converge, owing to the increase in $\delta(x_1^1 x_{P+1}^1)$ (which depends on $\langle x_1^2 x_{P+1}^2\rangle$).

However, the rough estimates above can underestimate drastically the cost of converging $\langle x_1^2 x_{P+1}^2\rangle$ since the ideal variance of the error should be at least an order of magnitude smaller than the characteristic amplitude of oscillations on $\langle x_1^n x_{P+1}^n\rangle$. We note that the amplitude of oscillations in $\langle x_1^2 x_{P+1}^2\rangle$ have an inverse relationship to the frequency ω^2, and so, if, for example, we used $\omega^2 = 1$ ($\beta = 8$), the amplitude of oscillation observed for $\langle x_1^2 x_{P+1}^2\rangle$ would be $\sim 10^{-4}$, suggesting that we should converge the integral to $\sim O(10^{-5})$. For this reason, we chose $\omega^2 = \frac{1}{8}$ for the harmonic oscillator example studied here since one gets comparable magnitudes for the amplitude of oscillation for $\langle x_1^n x_{P+1}^n\rangle, n = 1, 2$ ($n = 2$ is shown in Fig. 5). The top panel in Fig. 5 shows a measure of cost of converge $\varepsilon(n_{mc})$, as the difference between the converged correlation functions of $G_{x^n x^n}, n = 1, 2, 3$ and their values for different number of MC steps, across three orders of magnitude and averaged over 20 units of time. Here, we define

$$\varepsilon(n_{mc}) = \frac{1}{N_t}\sum_i^{N_t} \left| G_{x^n x^n}(t_i)^{n_{mc}} - G_{x^n x^n}(t_i)^{n_\infty} \right| / \bar{\sigma}_n, \qquad (29)$$

where

$$\bar{\sigma}_n = \frac{1}{N_t}\sum_i^{N_t} \left| G_{x^n x^n}(t_i)^{n_\infty} - \overline{G_{x^n x^n}} \right| \qquad (30)$$

and

$$\overline{G_{x^n x^n}} = \sum_i^{N_t} G_{x^n x^n}(t_i)^{n_\infty} / N_t.$$

Here, $\varepsilon(n_{mc})$ is the difference between the correlation function $G_{x^n x^n}$ after n_{mc} Monte Carlo integration and the converged $n_\infty \approx 10^9$ result, averaged over N_t equidistant time slices $0 \le t_i \le 20$. $\varepsilon(n_{mc})$ is also re-scaled by $\bar{\sigma}_n$, the standard deviation of the oscillations averaged over the same time domain so as to place the errors of these different correlation functions approximately on the same footing (this makes the scale in Fig. 5 arbitrary). It is worth noting that converging all TCFs at high temperatures is considerably easier, the number of samples being cut by at least an order of magnitude.

There is a clear difference in cost between $G_{x^n x^n}, n = 1, 3$ (blue cross and red filled square) and $n = 2$ (green circle). This

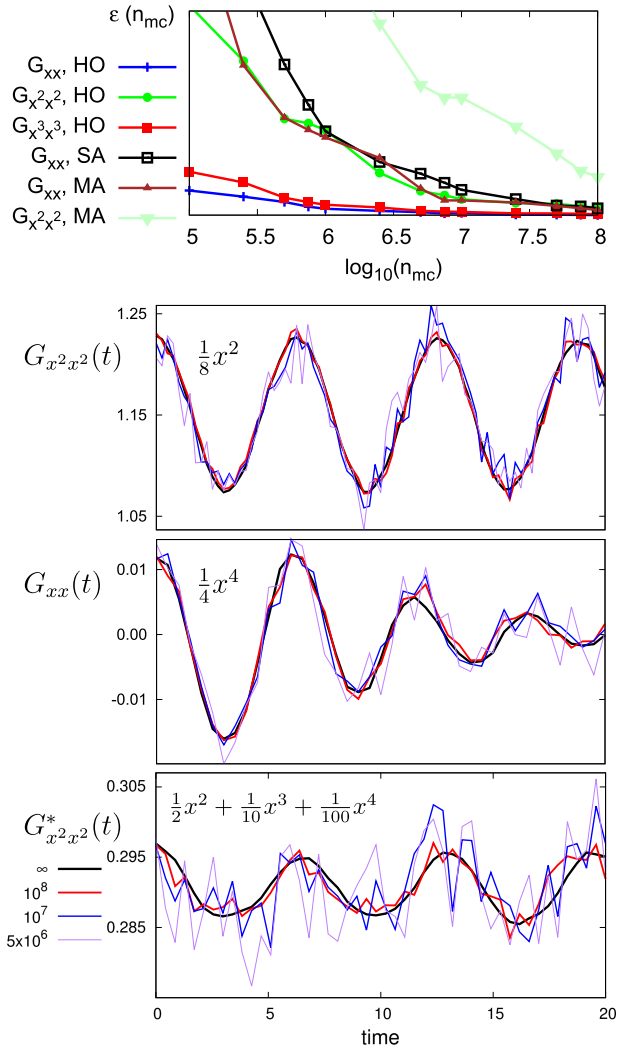

FIG. 5. (*Top*) Convergence of error [Eq. (29)] with respect to number of MC steps n_{mc} for different correlation functions of the models tested ($\beta = 8$, $2P = 80$), see text for details. *Legend*: HO: Harmonic Oscillator; SA: Strong Anharmonic; MA: Mild Anharmonic. Also shown are three of the more costly correlation functions from the top panel at different number of MC steps: $G_{x^2x^2}$ for $\frac{1}{8}x^2$ (*second from top*), G_{xx} for the strong (*second from bottom*), and $G_{x^2x^2}$ for the mildly (*bottom*) anharmonic models.

is partly due to the amplitude of oscillations being typically larger and can cross the y axis, so the coherence can be resolved "quicker." This difference in amplitude was partially addressed by the $\bar{\sigma}_n$-rescaling just described. To exhibit approximately the same relative error between $n = 1$ and $n = 2$, we require nearly two orders of magnitude number of samples. Despite this cost, with $10^{6.5}$ steps, one is already able to minimise the error sufficiently to exhibit oscillations, as can be seen for the harmonic oscillator in the second from the top panel of Fig. 5. The re-scaling for the monotonic error growth in $G_{x^2x^2}$ described in Subsection 1 of the Appendix was used to get a better estimate of convergence using Eq. (29) (though for $2P = 80$, it is only a small shift).

Also shown in Fig. 5 is the convergence of G_{xx} for the strongly anharmonic model (i.e., quartic oscillator, using D-fit) described in Sec. III C (but $2P = 80$, for better comparison) is also shown (black empty square). The cost of convergence is larger than that of any harmonic oscillator correlation function.

The rescaling by $\bar{\sigma}_n$ in this case slightly exaggerates the cost it takes to converge this correlation function, since the amplitude decreases towards zero as it approaches $t = 20$, leading to a larger error for "later" real-times. This can be seen in the second from the bottom panel of Fig. 5, which also shows the convergence for different number of MC steps; the "early" ($t < 10$) times are clearly resolved compared to later ones by $10^{6.5}$ MC steps.

Finally, the cost of convergence of $G_{x^{1|2}x^{1|2}}$ for the mildly anharmonic model is also shown in Fig. 5. Converging $G_{xx}(t)$ (brown up triangle) has approximately the same cost as that for the strongly anharmonic model (or $G_{x^2x^2}(t)$ for the harmonic oscillator). The most expensive of all correlations evaluated was $G_{x^2x^2}$ (sea green down triangle), for this mildly anharmonic model, which took $\sim 10^{9.5}$ samples to make it smooth (see the bottom panel). However, it is worth noting that despite the noise in the results, a clear coherence is observed by $\sim 10^8$, and maximum entropy analytic continuation (MEAC) techniques could then possibly be applied to this or $G_{x^2x^2}(t)$ to obtain a better approximation to the spectra.[54,90]

IV. DISCUSSION

The weighting function, F^-, gives importance to trajectories near the classical path [Eq. (21)], and in this sense, it is reminiscent to stationary phase filtering methods[85] or including sampling functions which weight away from highly oscillatory regions.[30,84] In fact, the first and most obvious way one would think to use $F^-(\mathbf{x}^+)$ would precisely be as an importance sampling function to weigh the sampled regions near the classical path, as shown in Eq. (21). However, our experiments in this direction to date [in other words, using $F^-(\mathbf{x}^+)$ as an additional importance sampling function with which to calculate $G_{AB}(t)$ using Eq. (3)] have not been successful. In particular, we find that using $F^-(\mathbf{x}^+)$ as an importance-sampling function fails to improve sampling in Eq. (3). The function $F^-(\mathbf{x}^+)$ only depends on the coordinates of the central "sum" string, while the dependence on the difference coordinates appears implicitly via the harmonic approximation of the PES. As a result, this importance sampling of the difference coordinates does not do enough to sufficiently alleviate the "sign problem" which appears in any scheme for calculating properties using Eq. (3).

The HPA-MC method, as proposed here, seems to suffer from inaccuracies at all times for anharmonic potential. These same symptoms are worst for the high temperature case ($\beta = 1$), where coherences are observed, but with the wrong frequencies for longer times, a problem which is also apparent in other standard methods.[22,58] For anharmonic potential containing odd terms, it was necessary to include a re-scaling factor in order to avoid a monotonic growth in the error for the position correlation functions. This also leads to a rapid decay of the G_{xx} autocorrelation function which makes the method inapplicable to study long time dynamics. The evaluation of $G_{x^2x^2}$ proved to be particularly costly, suggesting that better sampling techniques would be required if one desired to apply this approach to larger systems. Conceivably, the use of maximum entropy analytic continuation (MEAC) methods could improve the frequency-domain inversion required to obtain the spectra of the dynamical operator in question from this approximation.[82,90,91] The poor performance at high temperatures and long times can be in part traced to the loosening of the bead spring terms $\frac{mP\beta}{4|\tau|^2\hbar^2}$, which lead to a larger distances between of the forward and backward beads x, x' for which sum/difference coordinates are used. The harmonic interpolation of the potential for large $|x - x|'$ leads to a poorer estimation of the contribution of the phase to the TCF integral.

Equation (22) shows that integrating over the mixed temperature (imaginary time) and real time leads to a classical evolution which has a "memory" of the trajectory traversed, via the coupling matrix $((H^-)^{-1}_{ij})$, the covariance of the displacements along the difference coordinates. However, it is worth noting that the elements $((H^-)^{-1}_{iP}), 2 \leq i \leq P$ decay rapidly as $P - i$ increases, suggesting a limit to how the more distant evolution of x^+ beads affect the x^+_{P+1} bead. Developing approximations utilising this insight, together with the fact HPA-MC work for short times, are being investigated.

Further serious issues are likely to arise for systems whose potential exhibits points with negative curvature, such as transition state barriers, or PESs, such as the Morse function; in such cases, the Fourier transform along the difference coordinates is no longer well defined, and the expression in Eq. (19) [or (23)] would result in a poor representation of the integral. As a first approximation, it would be conceivable to set any negative curvatures present to zero and treat the coordinate as a free particle in such regions. It is also worth noting that similar problems arise in methods which rely on harmonic approximation of the PES in order to sample the thermal Wigner distribution.[76] In such cases, Miller and co-workers have proposed methods to approximately correct this by replacing imaginary eigenvalues with appropriate positive eigenvalues. We hope that such similar approaches might also be applicable in the context of HPA-MC, and work is ongoing in this direction.

If an interpolation/numerical derivative scheme which uses only potential energies were to be employed, then one could also perform MD or hybrid MD MC[19] to converge the integral, without the need to evaluate either gradients (if using MC) or second derivatives (if using MD). One can easily parallelise the integral evaluation for any real time t, as well as parallelising the sampling procedure (parallel Markov chains), an appealing feature of any algorithm. We can also expect this approach to be amenable to the inclusion of electronic state manifolds via Mayer-Miller mapping, which exactly maps the electronic degrees of freedom to harmonic oscillators.[92] Furthermore, since we are sampling from the correct density ρ, this approach is unlikely to suffer zero-point energy leakage.[8] Finally, it is also worth noting that higher-order path-integral discretisation schemes have also been used in the previous work;[93] in the case of PIMD simulations, such methods require knowledge of the Hessian, as in HPA-MC. As a result, it will be worth exploring how one might go about deriving HPA-MC starting from a higher-order representation of the Boltzmann operator; in addition, we are also interested in investigating how the interpolation schemes employed here might be used to derive approximate Hessian information for

higher-order PIMD simulations. Again, these issues remain for future work.

Despite the reasonable performance exhibited for 1D model problems at low temperatures, it remains to be seen whether this approach will work effectively with a larger number of degrees of freedom, as well as for systems coupled to some environment. A second-order expansion of a multi-dimensional potential with coupling terms would result in cross terms in the system Hessian. Such terms could be, for example, approximated by the numerical partial second derivatives from the ρ-sampled geometries. Similarly, a many-coordinate generalisation for obtaining temperature-dependent effective frequencies as described in Subsection III A, which one uses to generate a harmonic-phase normal representation is likely possible.

The principal bottleneck in the evaluation of F^- can be narrowed to calculate $(H^-)^{-1}$ [the generalisation of Eq. (A3)]. We therefore expect the cost of the algorithm to scale at most as $\mathcal{O}(n^3)\}$ with $n = PN$, where N is the number of system degrees of freedom. H^- can be shown to be no longer tridiagonal but can take a quasi-block diagonal (banded) form. The cost of inverting H^- would amount to the cost of inverting such blocks and the sparse matrix multiplication involving these,[94] thereby reducing the cost of matrix inversion. This method is more expensive than (linear-scaling) semiclassical methods that compute correlation functions, which only require classical trajectories sampling an initial distribution over phase-space. But, it will nevertheless be worth investigating how robust this approach is when applied to real problems.

V. CONCLUSIONS

From the standard position path-integral form of the symmetric complex correlation function, we employed the well-known sum/difference transformation between the beads in the forward and backward paths and introduced a harmonic approximation for the potential energy surface, resulting in a Gaussian weighting which can be used to approximately recover the coherence between the forward-backward paths. HPA-MC was used to study 1D model problems typically used in the literature. The correlation functions for harmonic systems are exact. Appealingly, it can in principle also provide time-correlation functions for non-linear operators, which can be required for the evaluation of a number of dynamical quantities,[95] such as measured, for example, incoherent dynamic structure factors during inelastic neutron scattering.[65] The method provides a reasonable approximation of linear and non-linear operator TCFs for anharmonic models, for short times and low temperatures, and should also be easily implemented in MD programs. The approximation is likely to maintain zero-point energies and could be easily applied to represent many-electron degrees of freedom. Despite these advantages, the approximation is unable to provide information for long real-times and high temperatures for anything other than harmonic oscillators. Nevertheless, it is the authors' hope that despite these shortcomings, the ideas presented here may lead to further approximations and algorithms that may overcome these limitations, some of which are currently underway.

ACKNOWLEDGMENTS

The authors gratefully acknowledge funding for this project by the Leverhulme Trust (No. RPG-2016-003). Computational resources were provided by the Scientific Computing Research Technology Platform at the University of Warwick. Data from Figs. 2–8 can be found at http://wrap.warwick.ac.uk/id/eprint/91744.

APPENDIX: ANALYSIS OF HPA-MC TCF FOR HARMONIC PESs

For a harmonic oscillator, the system potential separates the sum/difference coordinates exactly, and the x_1 and x_{P+1} coordinates are only coupled to the x^+ coordinates in ρ^+. If one wishes to evaluate the density $\int d\hat{x}\rho$, one needs only to sample the ρ^+ part, which contains only $P + 2$ x^+ coordinates, as opposed to $2P$. For TCF of operators involving purely x_1, x_{P+1} beads ρ^+ is a more succinct representation of the density, and all contribution from the phase arise from the integral $\int d\mathbf{q}^- \rho^- e^{i\Phi'} = F^-$, which depends solely on the x^+ coordinates and its derivatives. This observation motivated the HPA-MC approximation used in this article. For the harmonic oscillator model, the exponent in $\rho^+ F^-$ is quadratic in x^+, and the Hessian can be evaluated for once and for all t. We shall analyze the dependency correlation functions have on the systems variables β, t, m, P, and ω.

In what follows, we shall set $a = 1/\sqrt{2}$ so that all representations shown below will be related via rotations to the Cartesian coordinates. Though not immediately relevant to MC algorithms, this choice has some implications when considering MD methods of integration, and in particular, when considering how to provide "appropriate" masses to the kinetic energy of beads. Any choice other than $a = 1/\sqrt{2}$ makes the new coordinates unevenly stretch/compress the relative areas of the x, x' in phase-space. This results in the effective masses of the KE operator to be different to those of x_1^+ and x_{P+1}^+ (only labelled with + for convenience) and rotating to a diagonal Hessian (normal mode) representation from these scaled coordinates would lead to a non-diagonal KE operator.[83] Labelling the rotation representation $a = \frac{1}{\sqrt{2}}$ as $x^{\surd}$, to transform to it from any other choice of a, we must scale by $x^{\surd+} = a\sqrt{2}x^+$ and $x^{\surd-} = \sqrt{2}/2a x^-$. Define vector $\vec{d}_k$ in the basis of x^+ coordinates

$$\vec{d}_k = \sum_{i=1}^{P+1} d_{ki} x_k^+, \qquad d_{ki} = \begin{cases} 2, & i = k \\ -\alpha, & i = k-1 \\ -\gamma, & i = k+1 \\ 0, & |i-k| > 1 \end{cases}, \quad \alpha = \begin{cases} 1/a, & i = 1 \\ 1, & i > 1 \end{cases}, \quad \gamma = \begin{cases} 1/a, & i = P+1 \\ 1, & i < P+1, \end{cases} \tag{A1}$$

This vector can then simplify the expression in Eq. (19), so the variables in the exponent of $\ln(F^-) = \varphi$ [Eq. (19)] are then

$$\sum_{k=2}^{P} \frac{(C_k^+)^2}{(\lambda_k^-)^2 + (\frac{\tau\omega}{P})^2} = \sum_{k=2}^{P} \frac{(\sum_{i=2}^{P} U_{ki}^- \sum_{\alpha=1}^{P+1}(d_{i\alpha} - (\frac{\tau\omega}{P})^2\delta_{i\alpha})x_\alpha^+)^2}{(\lambda_k^-)^2 + (\frac{\tau\omega}{P})^2}$$
$$= \sum_{\alpha,\gamma=1}^{P+1} \sum_{i,j=2}^{P} x_\gamma^+(d_{i\gamma} - (\frac{\tau\omega}{P})^2\delta_{i\gamma})(\sum_{k=2}^{P} \frac{U_{ki}^- U_{kj}^-}{(\lambda_k^-)^2 + (\frac{\tau\omega}{P})^2})(d_{j\alpha} - (\frac{\tau\omega}{P})^2\delta_{j\alpha})x_\alpha^+, \tag{A2}$$

where φ can be broken into the sum of three matrices,

$$\varphi = \frac{mt^2P}{\tau^2\beta}(\mathbf{x}^+)^T\{\mathbf{D} - (\frac{\tau\omega}{P})^2\mathbf{F} + (\frac{\tau\omega}{P})^4\mathbf{H^{-1}}\}\mathbf{x}^+,$$
$$D_{ij} = (\sum_{k,l=2}^{P} d_{ki}(H^-)_{kl}^{-1}d_{lj}),$$
$$F_{ij} = (\sum_{k,l=2}^{P} d_{ki}, (H^-)_{kl}^{-1}\delta_{lj} + \delta_{ki}(H^-)_{kl}^{-1}d_{lj}) \tag{A3}$$
$$(H^-)_{kl}^{-1} = \sum_{i=2}^{P} \frac{U_{ik}^- U_{il}^-}{(\lambda_i^-)^2 + (\frac{\hbar\tau\omega}{P})^2}.$$

The eigenvalues of these also depend on P via the dimensions of the x^- beads, $P-1$. All three matrices depend on all system parameter via $\mathbf{H^-}$, the inverse of which can be shown to have analytic solutions.[96] Therefore, the problem has, in principle, an analytic solution. We shall here restrict ourselves to solutions via linear algebra; we can find the eigenvector representation which diagonalises both the Gaussian density and phases,

$$\frac{1}{2}(\mathbf{x}^+)^T\mathbf{R}^T\mathbf{R}(\frac{\beta mP}{2\hbar^2\tau^2}\mathbf{H}^+ + 2\varphi)\mathbf{R}^T\mathbf{R}\mathbf{x}^+ = \frac{1}{2}\mathbf{r}^T\Lambda\mathbf{r},$$
$$\Lambda_{ii} = \lambda_i^{\varphi+} = \sum_{\alpha,\gamma=1}^{P+1} \frac{mP\beta}{2\hbar^2\tau^2}(R_{\gamma i}H_{\gamma\alpha}^+R_{\alpha i}) \tag{A4}$$
$$+ \frac{2mPt^2}{\beta\hbar^2\tau^2}\left(R_{\gamma i}\left(D_{\gamma\alpha} - (\frac{\tau\omega}{P})^2F_{\gamma\alpha} + (\frac{\tau\omega}{P})^4(H^-)_{\gamma\alpha}^{-1}\right)R_{\alpha i}\right).$$

We defined the formally positive semidefinite $\lambda_i^{\varphi+}$ without a square to simplify notations.

1. Position correlation functions

To keep the problem tractable, we shall restrict ourselves to studying the position autocorrelation function $A = B = x^n$. From Eq. (A4), we can write down the correlation functions $G_{x^nx^n}$, to different orders n:

$$G_{xx} = \langle e^{-\varphi}\rho^+\rangle^{-1}\int d\mathbf{r}(\sum_{i,j=1}^{P+1} R_{1i}r_iR_{(P+1)j}r_j)e^{-\sum_{k=1}^{P+1}\lambda_k^{\varphi+}r_k^2/2} = \sum_{i=1}^{P+1}\frac{R_{1i}R_{(P+1)i}}{\lambda_i^{\varphi+}},$$
$$G_{x^2x^2} = \langle e^{-\varphi}\rho^+\rangle^{-1}\int d\mathbf{r}(\sum_{i,j,k,l=1}^{P+1} R_{1i}r_iR_{1j}r_jR_{(P+1)k}r_kR_{(P+1)l}r_l)e^{-\sum_{k=1}^{P+1}\lambda_k^{\varphi+}r_k^2/2}$$
$$= \sum_{i,j=1}^{P+1}(R_{1i}^2R_{(P+1)j}^2 + 2R_{1i}R_{(P+1)i}R_{1j}R_{(P+1)j})(\lambda_i^{\varphi+}\lambda_j^{\varphi+})^{-1},$$
$$G_{x^3x^3} = \sum_{i,j,k=1}^{P+1}(9R_{1i}^2R_{(P+1)i}^2(R_{1k}R_{(P+1)k}) + 6(R_{1i}R_{(P+1)i})(R_{1j}R_{(P+1)j})(R_{1k}R_{(P+1)k}))(\lambda_i^{\varphi+}\lambda_j^{\varphi+}\lambda_k^{\varphi+})^{-1}, \tag{A5}$$
$$G_{x^4x^4} = \sum_{i,j,k,l}^{P+1}\{9R_{1i}^2R_{1j}^2R_{(P+1)k}^2R_{(P+1)l}^2 + 56R_{1i}^2R_{(P+1)j}^2(R_{1k}R_{(P+1)k})(R_{1l}R_{(P+1)l})$$
$$+ 24(R_{1i}R_{(P+1)i})(R_{1j}R_{(P+1)j})(R_{1k}R_{(P+1)k})(R_{1l}R_{(P+1)l})\}(\lambda_i^{\varphi+}\lambda_j^{\varphi+}\lambda_k^{\varphi+}\lambda_l^{\varphi+})^{-1},$$

where $\langle e^{-\varphi}\rho^+\rangle = \prod_{i=1}^{P+1}\sqrt{\frac{2\pi}{\lambda_i^{\varphi+}}}$. Figure 6 shows sixteen distributions corresponding to $\langle e^{-\varphi}\rho^+\rangle$ for different values of P along $10 < t < 140$. Each distribution has been normalised to emphasize the linear relationship between the maxima of the distribution and P (discussed in Subsection 2 of the Appendix). The right-hand tail of each distribution drops sharply to zero and determines how far in t the expectation value of any operator can be estimated. Figure 7 shows a representative case of how G_{xx} and $G_{x^2x^2}$ behave as a function of t for $\beta = 5$, $\omega^2 = 1$, $P = 25$. The amplitude of G_{xx} gradually decreases as it reaches the right-hand tail of $\langle e^{-\varphi}\rho^+\rangle$ (lower panel), shown in black dashes and scaled. The oscillations in $G_{x^2x^2}$ (upper panel in Fig. 7) also decrease, but worse, it very quickly suffers from a severe non-oscillatory monotonic growth as t increases (see red, $P = 25$). The spectra obtained resulting from such errors is likely to be poor. This symptom can be obviously addressed by increasing P, as shown in the $P = 75$ case, but it does suggest that to obtain a good estimate, one might need approximately four times more beads than for G_{xx}. Alternatively, it was observed that evaluation of the autocorrelation

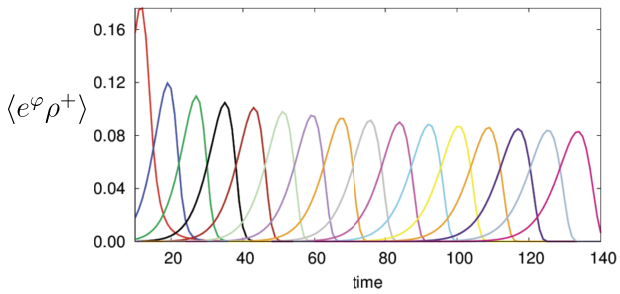

FIG. 6. $\langle e^{\varphi}\rho^{+}\rangle$ for sixteen values of P between $10 < t < 140$. Each distribution has been normalised to emphasize the linear relationship between the $\langle e^{\varphi}\rho^{+}\rangle$ maxima for a given P and t.

functions $(\langle x^2\rangle)^2$ or $(\langle x^4\rangle)$ suffer from precisely the same P-related growth of error as $G_{x^2x^2}$. A simple correction can be applied by multiplying $G_{x^2x^2}$ by $(\langle x^2\rangle)^2/(\langle x^2\rangle(t=0))^2$, which eliminates this error growth. The stared ($*$) blue $P = 25$ plot in the upper panel of Fig. 7 also shows the resulting correlation function; the amplitude now decays asymmetrically to the value of $(\langle x^4\rangle/3)$, but it is more susceptible to errors arising during Fourier transforms. $(\langle x^2\rangle)^2$ is a quantity which converges considerably quicker than its quartic counterparts and can therefore be obtained with some confidence. Since the growth in the error is due solely to the approximation in bead numbers, P, this re-scaling is also likely to work for non-harmonic potentials.

2. Choosing *P* for a given *t* in correlation functions

It is clearly important to have some idea of how P, the only free parameter in the approximation, should grow with t. The linear relationship between P and t and its effect on correlation functions (seen in Figs. 6 and 7) can be partially understood as the loss of correlation between adjacent beads in the ring by their weakening force constants as time increases.

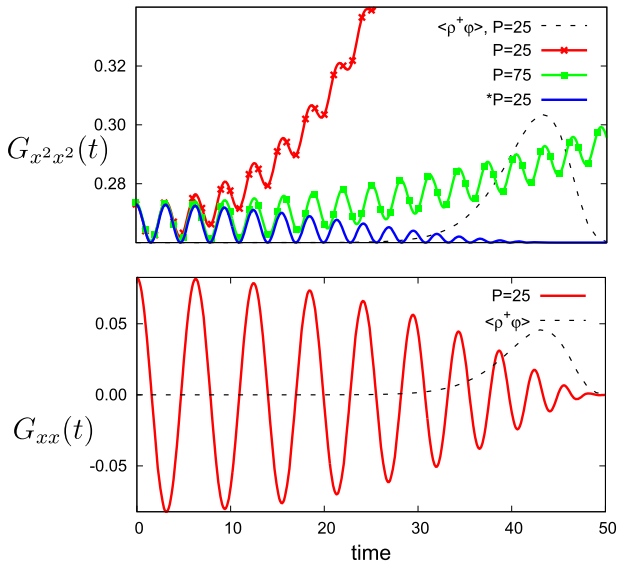

FIG. 7. Correlation functions G_{xx} (lower panel) $G_{x^2x^2}$ (upper panel) of $\omega^2 = 1, \beta = 5$ for $P = 25$ (red). Plot $P = 75$ (green) shows how the error in $G_{x^2x^2}$ has decreased. A corrective rescaling applied on $P = 25$ as described in text is shown in blue (upper panel). $\langle e^{-\varphi}\rho^{+}\rangle$ is also plotted (scaled and shifted) in black dashed lines to show the relationship to correlation functions.

Explicitly, in order to keep the normal-mode representation spring force constant $mP\beta\omega_r^2/4|\tau|^2\hbar^2$, where ω_r^2 corresponds to any of the ring eigenvalue forces ($0 \le \omega_r^2 \le 4$) and the system PI force constant $\beta\omega_s^2/2P$, where ω_s^2 corresponds to the harmonic oscillator's ("system") force constant, proportional, such that

$$\frac{mP\beta\omega_r^2}{4|\tau|^2\hbar^2} \propto \frac{\beta\omega_s^2}{2P} \tag{A6}$$

so that

$$P = \left\{\frac{2\omega_s^2}{\omega_r^2 m}(t^2 + \beta^2/4)\right\}^{\frac{1}{2}} \propto t. \tag{A7}$$

This suggests that, to guarantee that the ring spring constants do not become de-correlated, the number of beads need to be proportional to time (keeping $\frac{\tau}{P}$ roughly constant). In what follows, we shall concern ourselves in detail with parameters β and ω^2, and how these affect the proportionality between P and t. How the mass affects the required P shall be left for future work. Nevertheless, it is worth making an observation. A general potential does not have to depend on m so that it would also appear in the Hessian eigenvalue shifts in Eq. (A2) as $(\frac{\hbar\tau\omega}{\sqrt{mP}})^2$. Therefore m always appears multiplying P [Eq. (A2)], and, though P also affects the matrix size and therefore number of $\lambda^{\varphi+}$, it is likely to affect P inversely with the mass of the lightest particle of the system.

Given the close relationship between the sharp right-tail decay of $\langle e^{-\varphi}\rho^{+}\rangle$ and the correlation functions (Fig. 7), and the maxima of $\langle e^{-\varphi}\rho^{+}\rangle$ for a given P having a linear relationship with t (Fig. 6), we can estimate the number of beads required to obtain an approximate value for position correlation functions at some t. Parameters β and ω can affect the gradient and intercept of the aforementioned linear relationship,

$$P = \frac{dP}{dt}(\beta,\omega)t + P_0(\beta,\omega). \tag{A8}$$

We calculated grids of $\frac{dP}{dt}$ and P_0 for equidistant values of β and ω in the ranges $1 < \beta < 10$ and $0.5 < \omega^2 < 5.0$. We observed a near-linear behaviour in this region, for which we fitted the following functions for $\frac{dP}{dt}$ and $P_0(\beta,\omega)$:

$$\begin{aligned}\frac{dP}{dt}(\beta,\omega) &= \omega^2(0.232\,77 + \beta 0.005\,31) + 0.505\,87,\\ P_0(\beta,\omega) &= \omega^2 0.355\,44 + \beta 0.219\,90 + 0.450\,70.\end{aligned} \tag{A9}$$

The first equation shows that $\frac{dP}{dt}$ only depends on β as a function on ω. Figure 8 shows some $P(max(\langle e^{-\varphi}\rho^{+}\rangle(t)))$ v t plots for some values of β and ω^2. The strongest dependence is with respect to ω: larger values lead to larger P_0 and a steeper $\frac{dP}{dt}$,

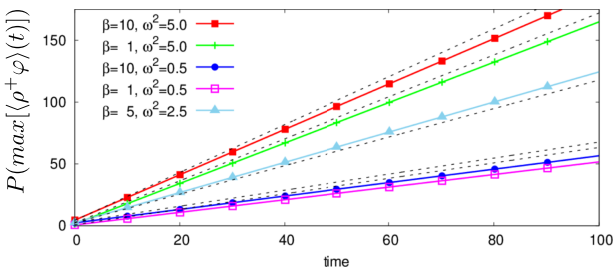

FIG. 8. The linear relationship between the P required to result give a maxima of the integral $\langle e^{-\varphi}\rho^{+}\rangle(t)$ for a given t, for different values of β, ω^2. The black dashes are the fitted linear model in Eq. (A9).

a similar but weaker trend was observed with respect to β. In black dashed lines in Fig. 8, we show the result of the fitted function in Eq. (A9), which approximately shows the correct behaviour. To get good results, however, one should in practice aim to have as many initial beads P_0 required for a reasonable convergence at time $t = 0$, which will be the same as that used for RPMD, $2P > \hbar\beta\omega_{max}$, where ω_{max} is the systems highest frequency. Furthermore, we suggest that in order to stay away from the decaying part of the correlation functions, it is best to also use a gradient ($\frac{dP}{dt}$) of at least twice the suggested value.

[1] R. P. Feynman and A. R. Hibbs, *Quantum Mechanics and Path Integrals* (McGraw-Hill, New York, 1965).
[2] D. Chandler, *Introduction to Modern Statistical Mechanics* (Oxford University Press, Oxford, UK, 1987).
[3] M. Parrinello and A. Rahman, J. Chem. Phys. **80**, 860 (1984).
[4] A. Wallqvist and B. Berne, Chem. Phys. Lett. **117**, 214 (1985).
[5] M. H. Alexander, Chem. Phys. Lett. **347**, 436 (2001).
[6] T. L. Beck, J. Chem. Phys. **96**, 7175 (1992).
[7] D. P. Geerke, S. Luber, K. H. Marti, and W. F. Van Gunsteren, J. Comput. Chem. **30**, 514 (2009).
[8] S. Habershon, T. E. Markland, and D. E. Manolopoulos, J. Chem. Phys. **131**, 024501 (2009).
[9] A. M. Reilly, S. Habershon, C. A. Morrison, and D. W. H. Rankin, J. Chem. Phys. **132**, 094502 (2010).
[10] A. M. Reilly, S. Habershon, C. A. Morrison, and D. W. H. Rankin, J. Chem. Phys. **132**, 134511 (2010).
[11] S. Habershon, Phys. Chem. Chem. Phys. **16**, 9154 (2014).
[12] T. Spura, C. John, S. Habershon, and T. D. Kühne, Mol. Phys. **113**, 808 (2015).
[13] A. Pérez and O. A. von Lilienfeld, J. Chem. Theory Comput. **7**, 2358 (2011).
[14] J. Gao, K.-Y. Wong, and D. T. Major, J. Comput. Chem. **29**, 514 (2008).
[15] R. Ramírez, C. P. Herrero, A. Antonelli, and E. R. Hernández, J. Chem. Phys. **129**, 064110 (2008).
[16] J. R. Schmidt and J. C. Tully, J. Chem. Phys. **127**, 094103 (2007).
[17] J. Morales and K. Singer, Mol. Phys. **73**, 873 (1991).
[18] R. P. Steele, J. Zwickl, P. Shushkov, and J. C. Tully, J. Chem. Phys. **134**, 074112 (2011).
[19] M. E. Tuckerman, B. J. Berne, G. J. Martyna, and M. L. Klein, J. Chem. Phys. **99**, 2796 (1993).
[20] J. Cao and G. A. Voth, J. Chem. Phys. **100**, 5106 (1994).
[21] D. Marx, M. E. Tuckerman, J. Hutter, and M. Parrinello, Nature **397**, 601 (1999).
[22] S. Bonella, M. Monteferrante, C. Pierleoni, and G. Ciccotti, J. Chem. Phys. **133**, 164104 (2010).
[23] N. Chakrabarti, T. Carrington, and B. Roux, Chem. Phys. Lett. **293**, 209 (1998).
[24] G. Krilov and B. J. Berne, J. Chem. Phys. **111**, 9147 (1999).
[25] J. D. Doll, J. Chem. Phys. **81**, 3536 (1984).
[26] J. D. Doll, R. D. Coalson, and D. L. Freeman, J. Chem. Phys. **87**, 1641 (1987).
[27] S. Habershon, G. S. Fanourgakis, and D. E. Manolopoulos, J. Chem. Phys. **129**, 074501 (2008).
[28] S. Habershon, J. Chem. Phys. **139**, 104107 (2013).
[29] T. D. Hone, P. J. Rossky, and G. A. Voth, J. Chem. Phys. **124**, 154103 (2006).
[30] N. Makri and W. H. Miller, Chem. Phys. Lett. **139**, 10 (1987).
[31] M. Topaler and N. Makri, J. Chem. Phys. **101**, 7500 (1994).
[32] E. Sim and N. Makri, J. Phys. Chem. B **101**, 5446 (1997).
[33] A. R. Menzeleev, F. Bell, and T. F. Miller III, J. Chem. Phys. **140**, 064103 (2014).
[34] M. Shiga and A. Nakayama, Chem. Phys. Lett. **451**, 175 (2008).
[35] G. A. Voth, Adv. Chem. Phys. **93**, 135 (2007).
[36] K. F. Wong, J. L. Sonnenberg, F. Paesani, T. Yamamoto, J. Vanícek, W. Zhang, H. B. Schlegel, D. A. Case, T. E. Cheatham, W. H. Miller, and G. A. Voth, J. Chem. Theory Comput. **6**, 2566 (2010).
[37] S. Jang and G. A. Voth, J. Chem. Phys. **111**, 2371 (1999).
[38] A. Witt, S. D. Ivanov, M. Shiga, H. Forbert, and D. Marx, J. Chem. Phys. **130**, 194510 (2009).
[39] V. Jadhao and N. Makri, J. Chem. Phys. **129**, 161102 (2008).
[40] N. Makri and W. H. Miller, J. Chem. Phys. **90**, 904 (1989).
[41] J. S. Shao and N. Makri, J. Phys. Chem. A **103**, 7753 (1999).
[42] H. Wang, X. Sun, and W. H. Miller, J. Chem. Phys. **108**, 9726 (1998).
[43] X. Sun, H. Wang, and W. H. Miller, J. Chem. Phys. **109**, 7064 (1998).
[44] X. Sun and W. H. Miller, J. Chem. Phys. **110**, 6635 (1999).
[45] W. H. Miller, J. Phys. Chem. A **105**, 2942 (2001).
[46] M. Thoss, H. Wang, and W. H. Miller, J. Chem. Phys. **114**, 9220 (2001).
[47] W. H. Miller, Proc. Natl. Acad. Sci. U. S. A. **102**, 6660 (2005).
[48] J. Liu, W. H. Miller, F. Paesani, W. Zhang, and D. A. Case, J. Chem. Phys. **131**, 164509 (2009).
[49] W. H. Miller, J. Phys. Chem. A **113**, 1405 (2009).
[50] J. O. Richardson and S. C. Althorpe, J. Chem. Phys. **131**, 214106 (2009).
[51] T. J. H. Hele and S. C. Althorpe, J. Chem. Phys. **138**, 084108 (2013).
[52] T. J. H. Hele, M. J. Willatt, A. Muolo, and S. C. Althorpe, J. Chem. Phys. **142**, 191101 (2015).
[53] N. Ananth, J. Chem. Phys. **139**, 124102 (2013).
[54] S. Habershon, B. J. Braams, and D. E. Manolopoulos, J. Chem. Phys. **127**, 174108 (2007).
[55] T. E. Markland, S. Habershon, and D. E. Manolopoulos, J. Chem. Phys. **128**, 194506 (2008).
[56] X. C. Huang, S. Habershon, and J. M. Bowman, Chem. Phys. Lett. **450**, 253 (2008).
[57] S. Habershon and D. E. Manolopoulos, J. Chem. Phys. **131**, 244518 (2009).
[58] S. Habershon, D. E. Manolopoulos, T. E. Markland, and T. F. Miller, Annu. Rev. Phys. Chem. **64**, 387 (2013).
[59] I. R. Craig and D. E. Manolopoulos, J. Chem. Phys. **121**, 3368 (2004).
[60] I. R. Craig and D. E. Manolopoulos, J. Chem. Phys. **122**, 084106 (2005).
[61] I. R. Craig and D. E. Manolopoulos, J. Chem. Phys. **123**, 034102 (2005).
[62] T. F. Miller and D. E. Manolopoulos, J. Chem. Phys. **123**, 154504 (2005).
[63] T. F. Miller and D. E. Manolopoulos, J. Chem. Phys. **122**, 184503 (2005).
[64] B. J. Braams and D. E. Manolopoulos, J. Chem. Phys. **125**, 124105 (2006).
[65] I. R. Craig and D. E. Manolopoulos, Chem. Phys. **322**, 236 (2006).
[66] R. Collepardo-Guevara, I. R. Craig, and D. E. Manolopoulos, J. Chem. Phys. **128**, 144502 (2008).
[67] A. R. Menzeleev and T. F. Miller, J. Chem. Phys. **132**, 034106 (2010).
[68] N. Boekelheide, R. Salomón-Ferrer, and T. F. Miller, Proc. Natl. Acad. Sci. U. S. A. **108**, 16159 (2011).
[69] A. R. Menzeleev, N. Ananth, and T. F. Miller, J. Chem. Phys. **135**, 074106 (2011).
[70] C. John, T. Spura, S. Habershon, and T. D. Kühne, Phys. Rev. E **93**, 043305 (2016).
[71] L. H. de la Pena and P. G. Kusalik, J. Chem. Phys. **121**, 5992 (2004).
[72] E. Geva, Q. Shi, and G. A. Voth, J. Chem. Phys. **115**, 9209 (2001).
[73] F. Paesani and G. A. Voth, J. Chem. Phys. **132**, 014105 (2010).
[74] W. H. Miller, J. Phys. Chem. B **106**, 8132 (2002).
[75] J. Liu and W. H. Miller, J. Chem. Phys. **127**, 114506 (2007).
[76] J. Liu and W. H. Miller, J. Chem. Phys. **131**, 074113 (2009).
[77] G. Tao and W. H. Miller, J. Phys. Chem. Lett. **1**, 891 (2010).
[78] M. Rossi, M. Ceriotti, and D. E. Manolopoulos, J. Chem. Phys. **140**, 234116 (2014).
[79] J. O. Richardson and M. Thoss, J. Chem. Phys. **139**, 031102 (2013).
[80] P. Huo and D. F. Coker, J. Chem. Phys. **135**, 201101 (2011).
[81] P. Schofield, Phys. Rev. Lett. **4**, 239 (1960).
[82] G. Krilov, E. Sim, and B. J. Berne, J. Chem. Phys. **114**, 1075 (2001).
[83] M. Tuckerman, *Statistical Mechanics: Theory and Molecular Simulation*, Oxford Graduate Texts (Oxford University Press, Oxford, 2010), p. xv, 696 p.
[84] J. D. Doll, D. L. Freeman, and M. J. Gillan, Chem. Phys. Lett. **143**, 277 (1988).
[85] V. S. Filinov, Nucl. Phys. B **271**, 717 (1986).
[86] S. Bonella and D. F. Coker, J. Chem. Phys. **122**, 194102 (2005).
[87] A. Horikoshi and K. Kinugawa, J. Chem. Phys. **122**, 174104 (2005).
[88] G. M. Torrie and J. P. Valleau, J. Comput. Phys. **23**, 187 (1977).
[89] M. Sprik, M. L. Klein, and D. Chandler, Phys. Rev. B **31**, 4234 (1985).
[90] E. Gallicchio and B. J. Berne, J. Chem. Phys. **105**, 7064 (1996).
[91] M. Jarrell and J. E. Gubernatis, Phys. Rep. **269**, 133 (1996).
[92] H. D. Meyer and W. H. Miller, J. Chem. Phys. **70**, 3214 (1979).
[93] S. Jang, S. Jang, and G. A. Voth, J. Chem. Phys. **115**, 7832 (2001).
[94] T. T. Lu and S. H. Shiou, Comput. Math. Appl. **43**, 119 (2002).
[95] D. A. McQuarrie, *Statistical Mechanics* (Viva Books Private Limited, New Delhi, 2003), p. 641.
[96] C. M. da Fonseca and J. Petronilho, Linear Algebra Appl. **325**, 7 (2001).